PHYSICAL REVIEW B **93**, 140101(R) (2016)

Electronic and magnetic properties of single Fe atoms on a CuN surface: Effects of electron correlations

S. K. Panda,[1] I. Di Marco,[1] O. Grånäs,[1,2] O. Eriksson,[1,*] and J. Fransson[1]

[1]*Department of Physics and Astronomy, Uppsala University, Box 516, SE-751 20 Uppsala, Sweden*

[2]*School of Engineering and Applied Sciences, Harvard, 29 Oxford Street, Cambridge, Massachusetts 02138, USA*

(Received 22 October 2015; revised manuscript received 22 February 2016; published 4 April 2016)

The electronic structure and magnetic properties of a single Fe adatom on a CuN surface have been studied using density functional theory in the local spin density approximation (LSDA), the LSDA+U approach, and the local density approximation plus dynamical mean-field theory (LDA+DMFT). The impurity problem in LDA+DMFT is solved through exact diagonalization and in the Hubbard-I approximation. The comparison of the one-particle spectral functions obtained from LSDA, LSDA+U, and LDA+DMFT show the importance of dynamical correlations for the electronic structure of this system. Most importantly, we focused on the magnetic anisotropy and found that neither LSDA nor LSDA+U can explain the measured high values of the axial and transverse anisotropy parameters. Instead, the spin excitation energies obtained from our LDA+DMFT approach with exact diagonalization agree significantly better with experimental data. This affirms the importance of treating fluctuating magnetic moments through a realistic many-body treatment when describing this class of nanomagnetic systems. Moreover, it facilitates insight to the role of the hybridization with surrounding orbitals.

DOI: 10.1103/PhysRevB.93.140101

Magnetic anisotropies are fundamental to understanding the nature of magnetic materials, nanodevices, and magnetic structures approaching the single-atom limit. As they are equally important for simple collinear and noncollinear magnetic structures in stabilizing the ground-state properties, anisotropic magnetic parameters have also been shown to be crucial for dynamical control of nonequilibrium quantities, e.g., magnetic resonances, switching phenomena, damping effects, and transport properties. Upon approaching the quantum limit, a full comprehensive and predictive theoretical framework for magnetism necessarily includes a quantum mechanical description of the local atomic environment.

In recent years much effort has been put into experimental studies of atomic-scale anisotropies using local probing, e.g., scanning tunneling microscopy/spectroscopy (STM/STS) [1–5], magnetic force microscopy [6], and mechanically controlled break junctions, as well as with averaging spectroscopy, e.g., angular/spin-resolved photoemission spectroscopy [7–9], x-ray magnetic circular dichroism (XMCD) [10–13], and x-ray absorption fine structure (XAFS) [14]. Theoretically, progress has been made using model Hamiltonians [15–21], density functional theory (DFT) [22–24], and more recently also by merging these two strategies [25]. It is well known that the model Hamiltonian can provide effective phenomenological theoretical descriptions whereas DFT is capable of reproducing ground-state properties, in principle without any experimental data as an input. Calculations based on single-reference DFT typically fail for materials with strong correlation, something that is within the capabilities of DMFT coupled to accurate electronic structure methods [26]. Such an LDA+DMFT approach has been very successful in addressing strongly correlated electron systems. However, typically, these calculations are aimed at describing bulk properties [26], while isolated paramagnetic defects have so far remained beyond reach. Hence most of the theoretical analysis of isolated adatoms on surfaces has been based on DFT using simple parametrizations of the exchange correlation functional, such as the local spin-density approximation (LSDA) and the generalized gradient approximation (GGA). There are some exceptions to this trend [25,27,28]. For example, in the recent work of Mazurenko *et al.* [25], spectral properties and exchange interactions of a transition-metal dimer deposited on a CuN surface were calculated through an Anderson impurity model, where dynamic correlation effects are considered, similar to LDA+DMFT.

So far there has been a large body of experimental investigations of magnetic nanostructures and adatoms on substrates. These studies involve, e.g., Co atoms on a Pt substrate [5], molecular magnets on a transition-metal substrate [29], and complex chiral magnetic structures of surfaces [30,31] and quantum corrals [32]. All these investigations have been analyzed theoretically, albeit only on an LSDA/GGA or LSDA+U level [29,33,34]. However, one may suspect that a theoretical treatment that goes beyond LSDA/GGA or LSDA+U would bring forth important effects that could explain, e.g., the too-small orbital moment of Co atoms on Pt [33] or the difficulty in describing the magnetic excitation spectrum of Fe on CuN [22]. The present work is focused on Fe adsorbed on CuN, as an archetype in this class of nanomagnetic systems. We address details of the electronic structure in relation to spectroscopic data and magnetic properties, and while we draw conclusions specific to this system (in light of Ref. [1]), we also analyze the implications of our results in more general terms. In this article we study a single paramagnetic adatom (Fe) on a surface (CuN), using a newly developed scheme based on DMFT combined with a full-potential linear muffin-tin orbital method (FP-LMTO) [35,36], and calculate all parameters pertaining to a quantum spin Hamiltonian and associated excitation spectrum. Our results show that correlation effects are in general important for this class of nanomagnets, both for electronic structure and magnetic properties.

*olle.eriksson@physics.uu.se

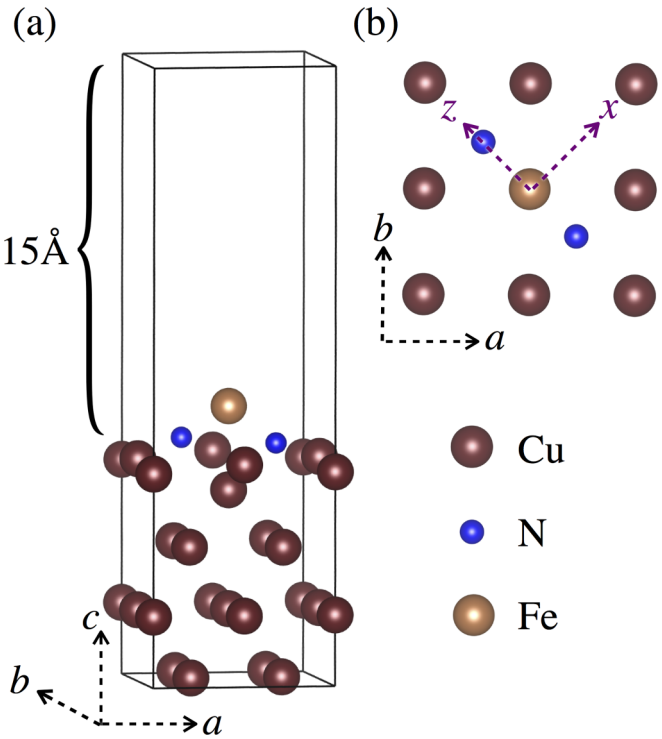

FIG. 1. (a) A schematic crystal structure of an Fe atom on a Cu(100)-c(2×2)N surface (2×2 supercell). (b) A top view of the structure, showing the local axes.

The experimentally reported structure of an Fe atom on Cu(100)-c(2×2)N surface has been simulated using a symmetric slab model, considering 2×2 and 4×4 supercells of 4 Cu(100) layers, including a 15-Å vacuum region. A schematic figure of the relaxed crystal structure of the 2×2 supercell is shown in Fig. 1(a). The N ions are distributed uniformly on the topmost layer with a 2:1 ratio and an Fe atom is adsorbed to the Cu site as reported in the STM study of Ref. [1]. We started our investigation by relaxing the ionic positions, using the projector augmented wave (PAW) method [37] as implemented in the Vienna *ab initio* simulation package (VASP) [38,39]. The relaxed geometry of both the supercells obtained in our calculations show that the adsorption of the Fe atom induces a local distortion on the surface, in good agreement with an earlier report [22]. The N atoms move upwards from the topmost Cu plane and the Cu atom just below the Fe ion is pushed downwards, making the Fe-Cu vertical distance around 2.3 Å. The distance between the Fe adatom and its nearest periodic image in the 2×2 supercell is 5.11 Å, while it is 10.22 Å in the 4×4 supercell. The top view of the structure is shown in Fig. 1(b), where the local x and z axes are respectively set along the (1 1 0) and (−1 1 0) directions. The y axis is chosen along the out-of-plane direction (0 0 1). This local frame is the same as the one used in Ref. [1], which will facilitate the comparison between experimental data and our results on the magnetic anisotropy.

The optimized structure has been used to analyze the electronic structure and the magnetic properties within LDA/LSDA, LSDA+U, and LDA+DMFT approaches using the FP-LMTO method [35,36] as implemented in the RSPt code [40]. The LDA+DMFT calculations of the paramagnetic phase are based on the implementation presented in Refs. [41–43]. The effective impurity problem for the Fe-3d states is solved through the exact diagonalization (ED) method [44] and also within the Hubbard I approximation (HIA) [45,46]. To describe the electron-electron correlation, we have assumed $U = 6$ eV and $J = 1.0$ eV for the Fe-d states, in agreement with a previous study [25]. Further technical details have been described in the Supplementary Material (SM) [47].

Before presenting our results, it is important to discuss the ideal size of the supercell needed to describe Fe adatoms on a CuN surface. In LSDA and LSDA+U one has to work with a symmetry-broken magnetic simulation, which may potentially lead to the formation of an artificial long-range order if the Fe atoms are too close. A good estimate of the interaction between the Fe atoms is given by the interatomic exchange interactions J_{ij}. We evaluate them from the converged LSDA+U calculations through the formalism of Ref. [48], and obtain 2.1 and 0.1 meV, respectively, for Fe atoms at interatomic distances of 5.11 and 10.22 Å. This implies that a 2×2 supercell is not enough to address this system and a 4×4 supercell must be considered. For the latter, the interactions are so small that there is no need to further increase the size of the supercell. The paramagnetic LDA+DMFT simulations do not require any broken symmetry, but a short Fe-Fe distance may affect the hybridization of the 3d states with all the other states. This can be measured through the hybridization function, which is the key quantity of DMFT and completely defines the effective impurity problem [26]. As shown in Fig. S1(a) of the SM, the hybridization function shows only minor changes between a 2×2 unit cell and 4×4 unit cell. Most importantly, these changes concern only the broadening of the peaks, and not their position or their weight [as shown by the integral in the inset of Fig. S1(a)]. Given that position and weight of the most important peaks are the only direct inputs of the exact diagonalization approach, we can perform the simulation with a 2×2 cell, which involves a much smaller computational effort.

We first look at the projected density of states (PDOS) obtained using LDA; see Fig. 2(a). The Fe-3d states are strongly m_l dependent and especially the curves for $m_l = \pm 2$ deviate from the corresponding plots for $m_l = \pm 1$ and $m_l = 0$ states. Despite these variations, all curves exhibit a peak near the Fermi level which is narrower if compared to bulk bcc Fe. This suggests that the 3d electrons are strongly localized here, which makes an LDA/LSDA-based approach inappropriate. The peak at the Fermi level emerges from the hybridization between the Fe adatom and the N-p states [Fig. 2(a)], and the hybridization strength is also different for different m_l-derived state, as confirmed by the hybridization function shown in the SM.

As mentioned above, LSDA and LSDA+U are not capable of describing fluctuating moments and therefore require a symmetry-broken magnetic solution. This induces a small but finite spurious magnetic moment in the atoms close to Fe. With this in mind we first inspect the PDOS obtained with LSDA and LSDA+U, reported in Fig. 2(b). Interestingly, the PDOS obtained in LSDA does not exhibit any gap at the Fermi level. Static correlation effects as in LSDA+U lead to a decrease of spectral weight at the Fermi level and to an extension of states

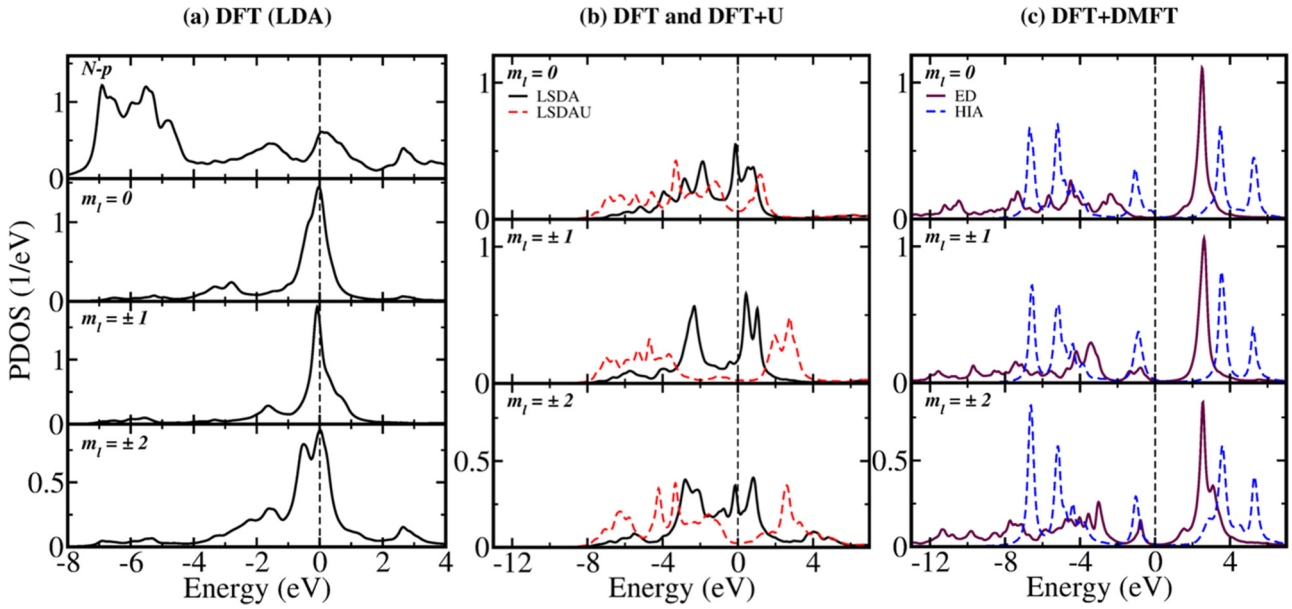

FIG. 2. PDOS for the Fe-3*d* orbitals as obtained from LDA (a), LSDA and LSDA+U (b), and LDA+DMFT with HIA and ED (c). For LDA also the N-*p* states are reported. The majority and minority PDOS are added for LSDA and LSDA+U.

over a broder range of energies. However, the spectrum is still gapless. In Fig. 2(c), we report the spectral function obtained in LDA+DMFT, which for simplicity we will also label as PDOS. We note that our paramagnetic LDA+DMFT results closely mimic the experimental scenario, since the system has only a single magnetic impurity with fluctuating local moments and no local Weiss field present. If no hybridization is considered, as in the HIA [46], a large gap arises and sharp peaks are present. As expected, the differences between the various m_l states are minor, because they originated mainly from the hybridization with the substrate. These effects are taken into account in LDA+DMFT with ED. In Fig. 2(c) one can see that the hybridization affects the different m_l projections to a different extent. In particular, in ED the band gap is decreased with respect to HIA, implying that the hybridization with the surface states shifts conduction and valence levels towards the Fermi level and the gap is different for different m_l states. These differences are reflected in the strong magnetic anisotropy, as discussed below. Interestingly, the formation of high-energy satellites in valence band spectra makes the ED spectrum much wider compared to all the other methods. The large differences obtained in LDA+DMFT with ED with respect to the other methods underlines the need for a proper treatment of correlation effects, hybridization, and magnetic order to address this class of nanomagnets.

Next we analyze the magnetic properties of this system, first as obtained from first-principle simulations and then in terms of an effective, quantum spin Hamiltonian. The computed energies, the Fe spin, and orbital moments, as well as the total moments per unit cell, are reported in Table I, for three different magnetization directions, as obtained from LSDA and LSDA+U with the inclusion of spin-orbit coupling (+SOC). Our calculations suggest that in both approaches the z axis (line of N ions) is the easy axis, which is in agreement with experiment [1] and with an earlier LSDA+SOC study [22]. Our calculations reveal that changing the magnetization direction does not affect the size of the Fe spin moment but significantly changes the orbital moment, which is greatest along the easy axis. Such a large orbital moment anisotropy is expected from the analysis of Ref. [49], where a direct proportionality between the orbital moment anisotropy and the magnetocrystalline anisotropy was derived. Table I also shows that both spin and orbital moments increase upon including static Coulomb corrections, as expected. The magnetic anisotropy parameters in LSDA+SOC and LSDA+U+SOC can be obtained by mapping the total energy differences between different magnetization axes (Table I) to the following spin Hamiltonian:

$$H = g\mu_B \mathbf{B}\cdot\mathbf{S} + DS_z^2 + E\left(S_x^2 - S_y^2\right). \quad (1)$$

Here, the first term corresponds to the Zeeman splitting due to the applied magnetic field **B**, while the second and third terms correspond to the axial and transverse anisotropy energies. Since Fe is very close to the d^6 atomiclike configuration, we can assume $S = 2$ in Eq. (1). The computed parameters (D and E) obtained from our calculations as well as previously reported theoretical and experimental values are shown in Table II. Our computed parameters within LSDA+SOC are larger compared to those reported by Shick *et al.* [22], who

TABLE I. Energy Δ_E, spin moment μ_s, orbital moment μ_o, and total cell moment $\mu_{\rm tot}$ for a given magnetization direction. The energy is relative to the energy of the cell with the magnetization along z.

	LSDA+SOC			LSDA+U+SOC		
	x axis	y axis	z axis	x axis	y axis	z axis
Δ_E (meV/cell)	2.46	1.42	0.00	3.58	1.80	0.00
μ_s (μ_B/Fe)	2.70	2.70	2.70	3.08	3.08	3.08
μ_o (μ_B/Fe)	0.02	0.06	0.16	0.03	0.10	0.21
$\mu_{\rm tot}$ (μ_B/cell)	3.50	3.53	3.64	3.74	3.80	3.92

TABLE II. Magnetic anisotropy parameters D and E, obtained through LSDA+SOC and LSDA+U+SOC, and compared to experimental data [1] and a previous theoretical study [22].

	LSDA+SOC (Ref. [22])	LSDA+SOC (this work)	LSDA+U+SOC (this work)	Exp. (Ref. [1])
D (meV)	−0.36	−0.48	−0.67	−1.55
E (meV)	0.10	0.13	0.22	0.31

considered a 2×2 supercell. For the sake of comparison we also considered a similar supercell and obtained $D = -0.32$ meV and $E = 0.09$ meV, which are in good agreement with Ref. [22]. These values correspond to a ∼50% reduction with respect to those obtained for a 4×4 supercell, which emphasizes the importance of considering an in-plane cell of adequate size. We also find that static Hartree-Fock corrections as described in LSDA+U increase the magnetic anisotropy considerably but not enough to explain the experimental data.

Finally we discuss the most important aspect of our study, the estimation of the spin excitation energies via LDA+DMFT. For this comparison it is particularly convenient to consider Eq. (1) in the absence of an external field. In this case, the axial term of the spin Hamiltonian [Eq. (1)] will split the degeneracy of the m_s projected states and the transverse term will mix them. Thus the degenerate $S = 2$ ground state will be split into five eigenstates, as schematically explained in Fig. 3. We can estimate the spin excitation energies for zero magnetic field by using D and E obtained from LSDA+SOC and LSDA+U+SOC (see Table II). The excited states can be marked as in Fig. 3. The energy differences with respect to the spin ground state ($|x_0\rangle$) are displayed in Table III. The LSDA+SOC values are significantly smaller than the experimental values reported in Ref. [1]. The electronic localization induced in LSDA+U+SOC leads to an increase of the spin excitation energies, but is not sufficient to reproduce

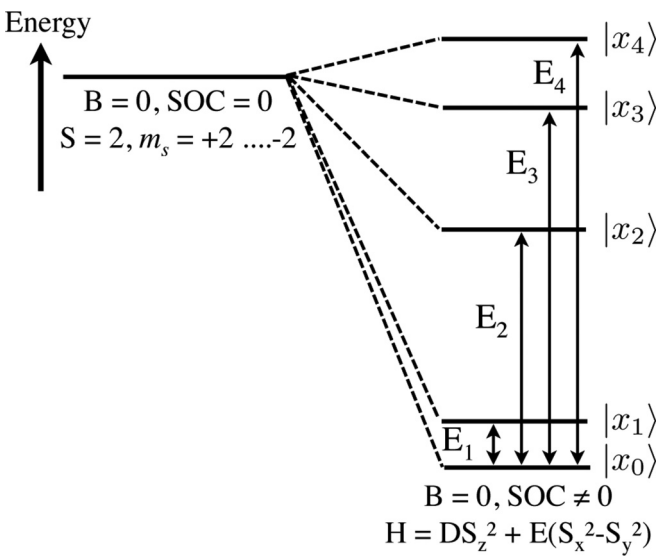

FIG. 3. Level diagram illustrating how a $S = 2$ degenerate ground state is split into five spin states due to spin-orbit coupling at zero magnetic field.

TABLE III. Spin excitation energies (in meV) as obtained within various approaches and compared to the experimental values from Ref. [1].

	E_1	E_2	E_3	E_4
LSDA+SOC	0.10	1.15	1.93	2.12
LSDA+U+SOC	0.20	1.55	2.87	3.08
LDA+DMFT+SOC (HIA)	0.03	12.08	12.23	13.76
LDA+DMFT+SOC (ED)	0.49	5.32	6.34	7.68
Experiment [1]	0.18	3.90	5.76	6.56

the experimental values. The tendency to underestimate the experimental response is likely to originate from the inability of these approaches to properly describe the formation of fluctuating local moments. These are instead fully accessible via LDA+DMFT+SOC. Further, in ED or HIA it is possible to extract the spin excitation energies directly from paramagnetic calculations. The many-body eigenstate $|\psi^{\mathbf{S}}_{\mathbf{i},\mathbf{m_S}}\rangle$ arising from the effective impurity can be indexed by $S(S+1) = \langle \mathbf{S^2} \rangle$ and $m_S = \langle S_z \rangle$. The eigenstates corresponding to $m_S = -S, \ldots, +S$ are degenerate in energy in the absence of SOC. The latter lifts the degeneracy and leads to a set of five eigenstates, which can be directly compared with the spin excitation energies. The values reported in Table III show that the energies obtained in LDA+DMFT+SOC in HIA are much larger than those obtained in LSDA+U+SOC, but also larger than the experimental values. As illustrated in the SM, these energies correspond to $D = -3.36$ meV and $E = 0.03$ meV, which are much different than the experimental data, as expected. The competition between the crystal field and local Coulomb interaction is well described by the HIA, which leads to the correct easy axis. However, this is not enough to obtain a full account of the spin-excitation spectra, as this requires including the hybridization with the environment, as in ED. This is due to the renormalized ligand field splitting as well as to the inclusion of charge fluctuations. Inspecting the thermally averaged d-orbital occupation (6.06 in HIA and 5.46 in ED), it is clear that charge fluctuations are more prominent in ED, with close to half-integer thermally averaged d occupation. This corroborates results from the parametrized impurity model by Ferrón *et al.*, who acquire the correct easy axis only when charge fluctuations are included [28]. Table III clearly shows the importance of the hybridization with the substrate in describing the spin excitation spectrum of Fe on CuN. The same conclusion is obtained if the spin-excitation energies are mapped into magnetic anisotropy parameters (see the SM). The obtained parameters $D = -1.84$ meV and $E = 0.18$ meV are in much better agreement with the experimental results than for all other methods (cf. Table II). From the discussion above it is clear that the effective spin Hamiltonian of Eq. (1) is rather efficient to parametrize the ED calculated excitation spectrum or the observed spectrum, where higher order terms are less important. This is in accord with the analysis of Yan *et al.* [50]. It is also relevant to mention here that Eq. (1) in conjunction with a transport model reproduces the spectra of a single Fe atom on CuN [51].

In conclusion, we have shown that magnetic order, dynamical correlation effects, and hybridization of the transition-metal atom with the surface states are very crucial to understanding

the electronic structure, magnetic properties, and spin excitation spectra of Fe on CuN. Static correlation effects as in the LSDA+U method fail to explain the large magnetic anisotropy energy observed, whereas the LDA+DMFT method describes magnetism of such materials with much improved accuracy. Our results suggest that LDA+DMFT with, e.g., ED is likely the method of choice to describe correlation effects for nanomagnets in general. In particular, all systems [4,20,52–54] with one or a few atoms on a substrate for which the DOS forms a narrow resonance of a few eV in width are expected to behave similarly to the presently investigated system.

This work was supported by the Swedish Research Council, the KAW Foundation (Grants No. 2012.0031 and No. 2013.0020), and eSSENCE. Calculations have been performed at the Swedish national computer centers UPPMAX and NSC.

[1] C. F. Hirjibehedin, C.-Y. Lin, A. F. Otte, M. Ternes, C. P. Lutz, B. A. Jones, and A. J. Heinrich, Science **317**, 1199 (2007).
[2] N. Tsukahara, K.-i. Noto, M. Ohara, S. Shiraki, N. Takagi, Y. Takata, J. Miyawaki, M. Taguchi, A. Chainani, S. Shin *et al.*, Phys. Rev. Lett. **102**, 167203 (2009).
[3] J. C. Oberg, M. R. Calvo, F. Delgado, M. Moro-Lagares, D. Serrate, D. Jacob, J. Fernández-Rossier, and C. F. Hirjibehedin, Nat. Nanotechnol. **9**, 64 (2013).
[4] I. G. Rau, S. Baumann, S. Rusponi, F. Donati, S. Stepanow, L. Gragnaniello, J. Dreiser, C. Piamonteze, F. Nolting, S. Gangopadhyay *et al.*, Science **344**, 988 (2014).
[5] Q. Dubout, F. Donati, C. Wäckerlin, F. Calleja, M. Etzkorn, A. Lehnert, L. Claude, P. Gambardella, and H. Brune, Phys. Rev. Lett. **114**, 106807 (2015).
[6] T. M. Nocera, J. Chen, C. B. Murray, and G. Agarwal, Nanotechnology **23**, 495704 (2012).
[7] M. Sawada, K. Hayashi, and A. Kakizaki, Phys. Rev. B **63**, 195407 (2001).
[8] M. Sawada, K. Hayashi, and A. Kakizaki, J. Phys. Soc. Jpn. **72**, 1161 (2003).
[9] R. Supruangnet, H. Nakajima, R. Chai-ngam, P. Songsiriritthigul, and A. Kakizaki, J. Phys. Soc. Jpn. **80**, 064706 (2011).
[10] C. Andersson, B. Sanyal, O. Eriksson, L. Nordström, O. Karis, D. Arvanitis, T. Konishi, E. Holub-Krappe, and J. H. Dunn, Phys. Rev. Lett. **99**, 177207 (2007).
[11] J. Honolka, A. A. Khajetoorians, V. Sessi, T. O. Wehling, S. Stepanow, J.-L. Mi, B. B. Iversen, T. Schlenk, J. Wiebe, N. B. Brookes *et al.*, Phys. Rev. Lett. **108**, 256811 (2012).
[12] T. Eelbo, M. Waśniowska, M. Sikora, M. Dobrzański, A. Kozłowski, A. Pulkin, G. Autès, I. Miotkowski, O. V. Yazyev, and R. Wiesendanger, Phys. Rev. B **89**, 104424 (2014).
[13] M. Ye, K. Kuroda, Y. Takeda, Y. Saitoh, K. Okamoto, S.-Y. Zhu, K. Shirai, K. Miyamoto, M. Arita, M. Nakatake *et al.*, J. Phys.: Condens. Matter **25**, 232201 (2013).
[14] A. Polyakov, H. L. Meyerheim, E. D. Crozier, R. A. Gordon, K. Mohseni, S. Roy, A. Ernst, M. G. Vergniory, X. Zubizarreta, M. M. Otrokov *et al.*, Phys. Rev. B **92**, 045423 (2015).
[15] J. Fransson, Nano Lett. **9**, 2414 (2009).
[16] J. Fernández-Rossier, Phys. Rev. Lett. **102**, 256802 (2009).
[17] J. Fransson, O. Eriksson, and A. V. Balatsky, Phys. Rev. B **81**, 115454 (2010).
[18] F. Delgado, J. J. Palacios, and J. Fernández-Rossier, Phys. Rev. Lett. **104**, 026601 (2010).
[19] B. Bryant, A. Spinelli, J. J. T. Wagenaar, M. Gerrits, and A. F. Otte, Phys. Rev. Lett. **111**, 127203 (2013).
[20] F. Donati, A. Singha, S. Stepanow, C. Wäckerlin, J. Dreiser, P. Gambardella, S. Rusponi, and H. Brune, Phys. Rev. Lett. **113**, 237201 (2014).
[21] P. Berggren and J. Fransson, Phys. Rev. B **91**, 205438 (2015).
[22] A. B. Shick, F. Máca, and A. I. Lichtenstein, Phys. Rev. B **79**, 172409 (2009).
[23] M. A. Barral, P. Roura-Bas, A. M. Llois, and A. A. Aligia, Phys. Rev. B **82**, 125438 (2010).
[24] O. Šipr, S. Bornemann, H. Ebert, S. Mankovsky, J. Vackář, and J. Minár, Phys. Rev. B **88**, 064411 (2013).
[25] V. V. Mazurenko, S. N. Iskakov, A. N. Rudenko, I. V. Kashin, O. M. Sotnikov, M. V. Valentyuk, and A. I. Lichtenstein, Phys. Rev. B **88**, 085112 (2013).
[26] G. Kotliar, S. Y. Savrasov, K. Haule, V. S. Oudovenko, O. Parcollet, and C. A. Marianetti, Rev. Mod. Phys. **78**, 865 (2006).
[27] A. Hurley, N. Baadji, and S. Sanvito, Phys. Rev. B **84**, 115435 (2011).
[28] A. Ferrón, J. L. Lado, and J. Fernández-Rossier, Phys. Rev. B **92**, 174407 (2015).
[29] A. Mugarza, R. Robles, C. Krull, R. Korytár, N. Lorente, and P. Gambardella, Phys. Rev. B **85**, 155437 (2012).
[30] M. Bode, M. Heide, K. von Bergmann, P. Ferriani, S. Heinze, G. Bihlmayer, A. Kubetzka, O. Pietzsch, S. Blügel, and R. Wiesendanger, Nature (London) **447**, 190 (2007).
[31] G. Chen, J. Zhu, A. Quesada, J. Li, A. T. N'Diaye, Y. Huo, T. P. Ma, Y. Chen, H. Y. Kwon, C. Won *et al.*, Phys. Rev. Lett. **110**, 177204 (2013).
[32] E. J. Heller, Nat. Phys. **4**, 443 (2008).
[33] P. Błoński and J. Hafner, J. Phys.: Condens. Matter **21**, 426001 (2009).
[34] V. S. Stepanyuk, L. Niebergall, W. Hergert, and P. Bruno, Phys. Rev. Lett. **94**, 187201 (2005).
[35] O. K. Andersen, Phys. Rev. B **12**, 3060 (1975).
[36] J. M. Wills and B. R. Cooper, Phys. Rev. B **36**, 3809 (1987).
[37] P. E. Blöchl, Phys. Rev. B **50**, 17953 (1994).
[38] G. Kresse and J. Hafner, Phys. Rev. B **47**, 558 (1993).
[39] G. Kresse and J. Furthmüller, Phys. Rev. B **54**, 11169 (1996).
[40] J. M. Wills, O. Eriksson, M. Alouni, and D. L. Price, *Electronic Structure and Physical Properties of Solids: The Uses of the LMTO Method* (Springer-Verlag, Berlin, 2000).
[41] A. Grechnev, I. Di Marco, M. I. Katsnelson, A. I. Lichtenstein, J. Wills, and O. Eriksson, Phys. Rev. B **76**, 035107 (2007).
[42] I. Di Marco, J. Minár, S. Chadov, M. I. Katsnelson, H. Ebert, and A. I. Lichtenstein, Phys. Rev. B **79**, 115111 (2009).
[43] O. Grånäs, I. Di Marco, P. Thunström, L. Nordström, O. Eriksson, T. Björkman, and J. Wills, Computat. Mater. Sci. **55**, 295 (2012).

[44] P. Thunström, I. Di Marco, and O. Eriksson, Phys. Rev. Lett. **109**, 186401 (2012).

[45] A. I. Lichtenstein and M. I. Katsnelson, Phys. Rev. B **57**, 6884 (1998).

[46] P. Thunström, I. Di Marco, A. Grechnev, S. Lebègue, M. I. Katsnelson, A. Svane, and O. Eriksson, Phys. Rev. B **79**, 165104 (2009).

[47] See Supplemental Material at http://link.aps.org/supplemental/10.1103/PhysRevB.93.140101 for computational details, hybridization function, and technical aspects of the anisotropy parameters calculations from the spin-excitation energies.

[48] Y. O. Kvashnin, O. Grånäs, I. Di Marco, M. I. Katsnelson, A. I. Lichtenstein, and O. Eriksson, Phys. Rev. B **91**, 125133 (2015).

[49] P. Bruno, Phys. Rev. B **39**, 865 (1989).

[50] S. Yan, D.-J. Choi, J. A. J. Burgess, S. Rolf-Pissarczyk, and S. Loth, Nano Lett. **15**, 1938 (2015).

[51] M. Ternes, New J. Phys. **17**, 063016 (2015).

[52] L. Zhou, J. Wiebe, S. Lounis, E. Vedmedenko, F. Meier, S. Blügel, P. H. Dederichs, and R. Wiesendanger, Nat. Phys. **6**, 187 (2010).

[53] A. A. Khajetoorians, J. Wiebe, B. Chilian, S. Lounis, S. Blügel, and R. Wiesendanger, Nat. Phys. **8**, 497 (2012).

[54] T. Miyamachi, T. Schuh, T. Märkl, C. Bresch, T. Balashov, A. Stöhr, C. Karlewski, S. André, M. Marthaler, M. Hoffmann *et al.*, Nature (London) **503**, 242 (2013).